Gas temperature dependence of particle-beam-pumped atomic xenon laser output

H. Tomizawa,* M. Salvermoser,* J. Wieser,** and A. Ulrich****

**Japan Synchrotron Radiation Research Institute (SPring-8), Kouto 1-1-1, Mikazuki, Sayo, Hyogo 679-5198, Japan*
***Fakultät für Physik E12, Technische Universität München, James-Franck str. 1, D-85747 Garching, Germany*
****Department of Physics, Rutgers University, Newark, New Jersey 07102, USA*

Received October 7, 2001

The influence of gas temperature on the output power and pulse shape of the 1.73 ($5d[3/2]_1$–$6p[5/2]_2$) and 2.03 μm ($5d[3/2]_1$–$6p[3/2]_2$) Xe I laser was studied. The laser gases were mixtures of a 0.3 and a 0.5% xenon concentration in 330 mbar argon buffer gases. In one experiment, 100 mbar helium was added. The laser was pumped using a pulsed 100 MeV $^{32}S^{9+}$ ion beam. Beam pulses were 30 and 50 μs-long of constant intensity and had rise and fall times of less than 100 ns. Temperature dependence of the laser output was measured. A titanium gas purifier was used to avoid the influence of impurities on the measurement. Water vapor density, in particular, was kept below 10^{13} cm^{-3}. A decrease of laser output power with increasing temperature was observed. Optical cavity losses were minimized in order to perform experiments over a wide range of gas temperatures (303 ~ 663 K) without going below laser threshold. Gas density was kept constant during the measurement. Adding helium to the laser gas mixture improved laser performance. Extreme afterglow lasing, reaching more than 20% of the entire energy in the 50 μs laser output and lasting for more than 20 μs, was observed in the temperature range between 392 and 553 K at a gas density of 6.7 ~ 5.0×10^{18} cm^{-3}. μ sing a broadband optical cavity and a gas mixture of 300 mbar argon gas with 1% xenon admixture, pumped by 20 μs beam pulses, competition between the laser lines at 1.73 and 2.03 μm with a complex time structure was observed.

Introduction

Direct conversion of nuclear energy to laser optical energy was considered as early as 1961 (Ref. 1). Nuclear pumped lasers (NPLs) have been intensively studied and developed in the USA and Russia since the first operation of a He–Xe NPL in 1972 (Refs. 2 and 3). Many different gas mixtures were used for NPLs in early experiments but failed. However, there have been successes using atomic rare gas mixtures for NPLs. One such success, which shows to be the most promising NPL in the near infrared region for high power applications,4 is the use of a 1.73 Um laser line in xenon atoms. Many experiments have been performed on the 1.73 Um line of xenon using an Ar–Xe gas mixture with total pressures ranging from 0.5 to 4 atm and a xenon gas content of 0.1–1% (Refs. 1–11). This laser has a high efficiency of max. 8% (Refs. 5–7) and a low threshold.1,8 It is a potentially high energy (up to 50 kJ) NPL with pulse lengths of around 10 ms (Ref. 9).

Despite the promising characteristics for high power applications, problems with atomic rare gas NPLs have become well known. Premature terminations of the laser output pulse seem to have occurred when high pumping-power density was used. Often, peak laser intensity is reached before the peak of the pumping power.[13–14] The problem of limited laser pulse reproducibility suggests the presence of factors that strongly influence the performance of the laser, but how these factors influence laser performance is not clearly understood. Several reasons for these NPL-problems have been discussed, and two main causes have been proposed to explain these phenomena.

Up to now, most experiments and their analysis have dealt with the temperature dependence of the Ar–Xe laser. Electron collisional mixing (ECM) has been suggested[10] as a cause of the temperature dependence. On the other hand, A.A. Mavlyutov et al. discussed the influence of water molecule impurities in the laser gas mixture on the intensity of the atomic xenon laser and performed experiments on this issue.[16] H. Tomizawa et al. demonstrated and quantitatively modeled electron attachment and collisional quenching with desorbing water vapor hazard laser oscillation.[17]

Modeling gas temperature dependence with the analytical method is very complicated. Most of the modeling of this effect is studied with numerical calculation. These numerical models need many parameters to accurately reproduce the shape of the laser output pulses. Some temperature dependence experiments have been performed over the last decade.[18–20] However, it seems that there is not yet

enough data to estimate unknown parameters for accurate numerical computation of laser gas kinetics.

Experiments have been performed to study the influence of the gas temperature of the laser gas mixture and its effects on the output power of the atomic xenon laser at a fixed gas pressure and density. In the experiments, all the other parameters of the laser were kept fixed. Herein, we present data that can be useful for testing time-dependent numerical models that reproduce laser pulse shapes.

1. Experiment

1.1. Experimental concept and setup

Experiments were performed using a beam of 100 MeV $^{32}S^{9+}$ heavy ions from the Munich Tandem van de Graff accelerator for the pumping of the Ar–Xe laser. The 30 and 50 Us-long beam pulses were applied at repetition rates of 30 and 33 Hz, respectively. Pumping power density was on the order of 100 W/cm^3 for a typical volume. The heavy ion beam pumping used here is a model system for the so-called NPL, which is pumped by fission fragments. An electrostatic chopper installed at the low energy side of the accelerator formed the beam pulses. This chopper can form rectangular beam pulses with rise and fall times of less than 100 ns (see Fig. 2). The use of these rectangular beam pulses is ideal for experiments studying NPLs and other recombination lasers. This is because the onset and afterglow of lasing can be measured precisely at the intermediate time in which a constant pumping power density has been achieved and an equilibrium state has occurred. The optical setup of the laser, schematically shown in Fig. 1, was similar to previous experiments performed at the Munich Tandem Accelerator.[17,21] The laser cell was built using standard stainless steel high vacuum components with a 100 mm inner diameter. The cell was separated from the beam-line of the accelerator by a 1 mg/cm^2 titanium entrance foil with a 4 mm aperture diameter. This entrance foil allowed for the maintenance of an atmospheric laser gas mixture in the cell and, at the same time, a vacuum pressure of less than 10^{-6} mbar in the beam line.

The optical axis of the laser was tilted, with respect to the ion beam axis, at an angle at which the laser output power reached its maximum. Two kinds of stable optical cavities were used, consisting of narrow-band (1.73 Um) dielectric and broadband gold-coated mirrors, respectively. The narrow-band laser mirrors had curvature radii of 1.5 and 10 m. Both broadband laser mirrors had a curvature radius of 4 m. The distance between the mirrors of both optical cavities was 70 cm.

Laser power was detected by measuring the output power reflected from the Brewster window (see Fig. 1). The detector was a germanium photodiode. It was tested for linear response up to a laser power of 10 mW. A correction factor was determined for accurately measuring laser output power of more than 10 mW. A small (15 cm-long) grating monochrometor was used to measure laser output of different lines separately when the broadband cavity was used.

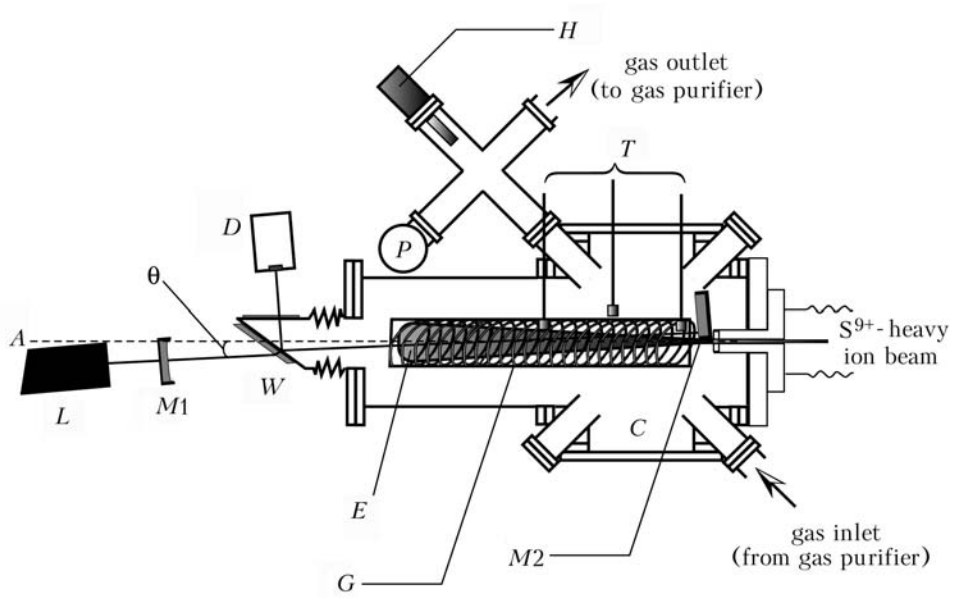

Fig. 1. Schematic drawing of the experimental setup. Shown above are the gas cell C, gas heater cell G, beam line, excited region E, laser optics (alignment laser L; mirrors $M1$ and $M2$ (rcc = 1.5 and 10 m); Brewster window W), pressure gauges P, germanium photodiode detector D, hygrometer H, and platinum resistance thermometer T. The angle that measured between the ion beam and laser axes was 1.2°.

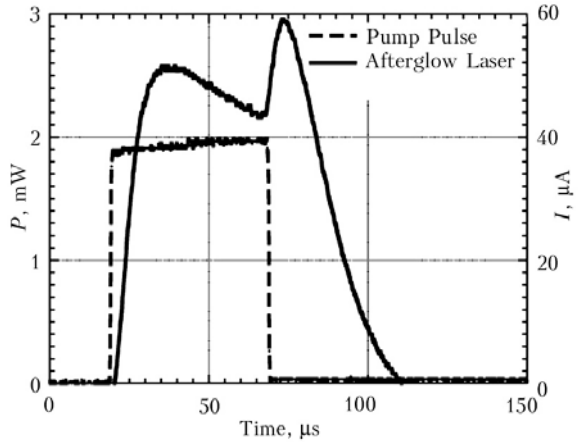

Fig. 2. Laser pulse observed in the gas temperature region between 392 and 553 K: Time dependence of laser output power P (solid line) at a gas temperature of 454 K and a gas density of 5.5×10^{18} cm^{-3}, and pump pulse intensity I (dotted line) for a pulse width of 50 μs are shown. The beam current of about 40 μA corresponds to a pumping power of 440 W.

The gas heater cell consisted of a 25 cm-long quartz cylinder with an inner diameter of 2 cm and a tungsten coil. This cell was installed in the gas cell to cover the overlap region of the active volume exiting from the heavy ion beam and laser mode volume. As long as the gas density stayed the same in the cell, the state of this overlap region was also kept constant. The gas temperatures of the inside (at the end and in the middle) and the outside of the gas heater cell were measured using platinum resistance thermometers.

The absolute total pressure of the laser gas mixture was measured using a capacitance manometer (Baratron, Type: 390HA-01000), with a sensor for a pressure range from 10^{-3} mbar to 1 bar with a reading accuracy to 0.15%. The laser gases were mixed using helium, argon, and xenon with a minimum purity of 99.998%. Mixtures of 330-mbar argon buffer gas containing 0.3 and 0.5% xenon were used as the laser gas. Some experiments were performed with an additional admixture of 100-mbar helium. All mixtures were prepared at room temperature. A closed gas system with a rare gas purifier operating with hot (1100 K) titanium was used. The gas mixture could be circulated through the gas cell and the purifier by a metal bellows compressor. Purification of the laser gas mixture is essential, especially as a prerequisite for measuring the influence of gas temperature independent from any other impurity effects, which may be caused by outgassing from the walls of the laser cell. Using a sensitive electrical hygrometer (Panametrics, Model 708E), water vapor density was carefully monitored during the experiments. Our purification system was capable of keeping outgassing at below 5×10^{13} cm^{-3} water vapor density at 663 K of the maximal gas temperature. It was observed[17] that the influence of water vapor on the laser output becomes significant for water vapor densities of more than 1×10^{13} cm^{-3}.

1.2. Experimental procedure

When performing this experiment, all parameters of the laser, except for gas temperature and gas density or pressure, should be kept constant. In particular, it is important to keep the lasing gas mixture free of water vapor in the gas heater cell.

In the first experiments, a narrow-band optical cavity was used while the laser gas in the gas heater cell was heated up to its maximum temperature, actively purifying the gas of water vapor and allowing for the measurement of water vapor densities by a hygrometer. Monitoring its concentration with the hygrometer, the gas was kept at a maximum temperature until the gas purifier had removed the water vapor from the laser gas. When the gas mixture contained less than 1×10^{13} cm^{-3} of water vapor, the heater current was reduced gradually while measuring the gas temperature with platinum resistance thermometers. The corresponding laser output was measured with the photodiode. Experiments were either performed at a constant gas density or total gas pressure. At the end of each temperature measurement run, gas temperature was brought back to room temperature. By this procedure, it was assured that only gas temperature affected the laser outputs at a gas density.

The second experiment was performed in the same way using a broadband optical cavity. A beam with a 20 Us pulse width at a repetition rate of 176 Hz was used. Laser output was measured through the monochrometor at 1.73 and 2.03 Um separately. Note that the 1.73 and 2.03 Um lines have a common upper laser level in a manifold of the Xe I laser. In the experiment for the Xe I laser, if one uses gold-coated mirrors for the cavity, it is possible to operate other laser lines, e.g., at 2.63, 2.65, and 3.3 Um, at the same time. The quartz glass window used here, however, acts as a filter for wavelengths longer than 2.60 Um. Consequently, no lasing was observed at those laser lines.

In all experimental runs, the intensity of the heavy ion beam was kept constant. Measurements were performed whenever both the laser output power and thermometer reading had stabilized.

As a preparation for these principle experiments, the influence of the magnetic field induced by the solenoid coil of the gas heater cell (see Fig. 1) was checked using an external copper coil around the outside of the cell. An influence of the magnetic field on the laser output or laser shape could not be observed over the gas temperature region studied. In order to avoid induced magnetic fields from the onset, the experiment using a broadband cavity was performed using a gas heater coil made of a recursive coaxial tungsten filament.

2. Experimental results

There are two series of experimental results using narrow-band or broadband cavities. The absolute values

of the laser output power were calculated from the proper calibration curve of a germanium detector. The error bars shown in the figures were due to the energy vibration of a heavy ion beam.

Our experimental setup achieved low optical cavity loss in order to perform experiments over a wide range of gas temperatures (303 ~ 663 K) without observing laser threshold. The maximum gas temperature difference between the middle and the edge of the overlap region in the gas heater cell was 10 K. The heavy ion beam pulses additionally raised the gas temperature on impact just during its pumping time in its active volume alone. In our experiments with constant density, additionally raised gas temperature by the heavy ion beam pulses is about 100 K. Thus, the temperature difference in the heater cell is ignitable. Note that the gas temperatures written in this paper are the measured gas temperatures in the gas heater cell.

Figure 2 shows the time dependence of the laser output pulse in the afterglow lasing part, in comparison to a 50 Us pump pulse. The data show that 2.5 Us is the offset time between the laser output pulse and the rectangular pumping power pulse.

The gas temperature dependences of the laser output powers at 1.73 Um using the narrow-band cavity are shown in Figs. 2–9. Note that the experimental data in Figs. 3 to 6 show the gas temperature dependence of the laser outputs alone, since the experiments were performed at a constant gas density by controlling gas pressure for the gas temperature. Lasing competitions between 1.73 and 2.03 Um lines at a high gas temperature are shown in Fig. 10.

2.1. Temperature dependence of laser output at 1.73 μm

Initially, laser pulses and output power using a purified Ar–Xe (0.3%) gas mixture with a constant density of $4.30 \pm 0.15 \times 10^{18}$ cm^{-3} pumped by 30 Us pulses are described. Examples of the laser output pulses at different gas temperatures are shown in Fig. 3. Note that the shape of the laser output pulses changes with the gas temperature. Maximum laser output power pumped by 30 and 50 Us pulse vs. gas temperature is shown in Fig. 4. Here, maximum laser output power means the averaged laser output power in the plateau region of the laser pulse. The error bars shown are the peak-to-peak fluctuation of the laser output power in its plateau region. The sets of two experimental data in Fig. 4 do not show any significant difference in thermal effects between 30 and 50 Us pumping beam pulses. The data show a significant linear reduction of laser output power in the region up to around 400 K, and an almost constant laser output with little reduction in the region from around 400 to 600 K.

After adding helium to this gas mixture, the laser output was studied for a purified Ar (76.4%) – He (23.4%) – Xe (0.3%) gas mixture with a constant density of $5.50 \pm 0.15 \times 10^{18}$ cm^{-3} pumped by 50 Us pulses. Examples of the laser pulses at different gas temperatures are shown in Fig. 5. Note that the shape of the laser output pulses changes with the gas temperature. Laser output power vs. gas temperature is shown in Fig. 6. The experimental data in Fig. 6 show an essentially linear reduction of laser output in the temperature region studied. A comparison of Figs. 4 and 6 shows that adding helium to the laser gas mixture improved laser performance.

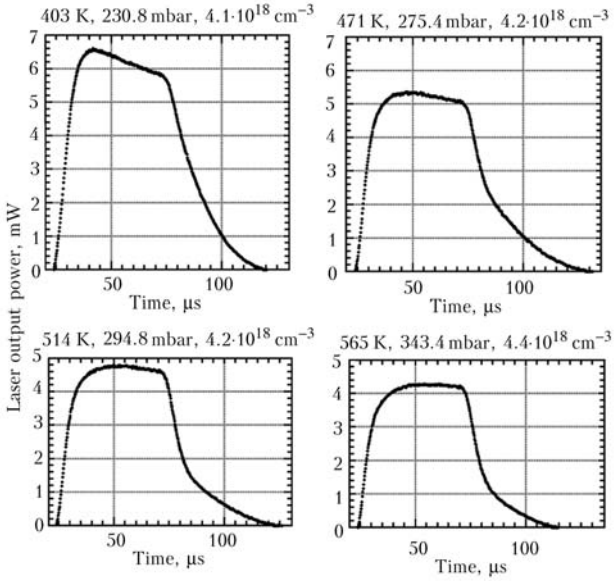

Fig. 3. Laser output power (mW) vs. time (μs) at the different gas temperatures in the gas heater cell. The laser gas was a mixture of 99.7% Ar and 0.3% Xe with $4.30 \pm 0.15 \times 10^{18}$ cm^{-3} of a constant density pumped by a 30 μs pulse. All other parameters, such as water vapor density, optical geometry, etc., were kept fixed.

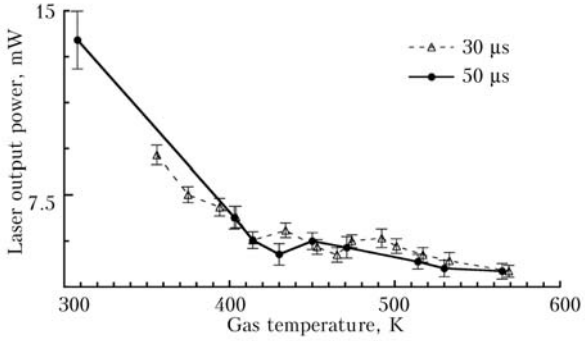

Fig. 4. Maximum power of laser output (mW) vs. gas temperature in the gas heater cell (K). The laser gas was a mixture of 99.7% Ar and 0.3% Xe with $4.30 \pm 0.15 \times 10^{18}$ cm^{-3} of a constant density pumped by a 30 and 50 μs pulse. All other parameters, such as water vapor density, optical geometry, etc., were kept fixed.

Next, data from another run show the laser output power using a purified Ar–Xe (0.3%) gas mixture for a constant gas pressure of 340 ± 2 mbar pumped by 30 and 50 Us pulses. Laser pulses pumped by a 30 and 50 Us pulse at different gas temperatures are shown in

Figs. 7*a* and *b*, respectively. Note that the laser output pulses change significantly at different gas temperatures. The laser pulse in power shows a pronounced afterglow. Up to around 400 K, the laser output pulses are constantly reduced. In this first temperature region, the laser pulses consist of only an ordinary lasing part. The afterglow lasing appears in the laser pulses only in the case of gas temperatures between 392 K and 553 K and gas densities between 5.0 and 6.7×10^{18} cm^{-3}. The afterglow lasing part grew from around 400 K, reached its maximum at around 450 K, and was reduced again at around 500 K. In this second temperature region, the higher the peak power of the afterglow lasing part of the laser outputs, the lower the power of the plateau region of the ordinary lasing parts becomes.

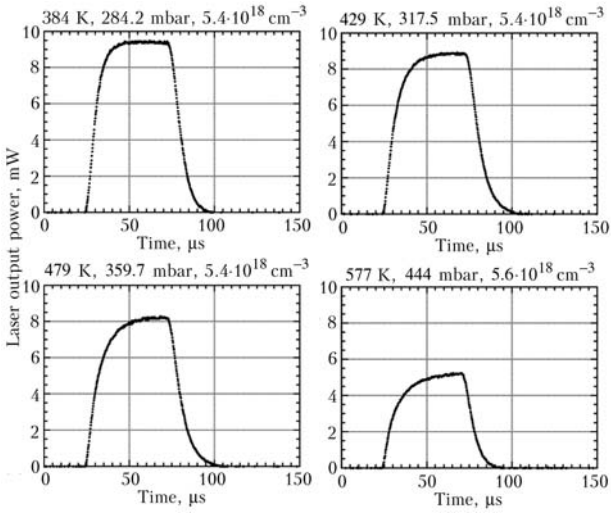

Fig. 5. Laser output power (mW) vs. time (μs) at the different gas temperatures in the gas heater cell. The laser gas was a mixture of 76.4% Ar, 23.4% He, and 0.2% Xe with $5.50 \pm 0.15 \times10^{18}$ cm^{-3} of a constant density pumped by a 50 μs pulse. All other parameters, such as water vapor density, optical geometry, etc., were kept fixed.

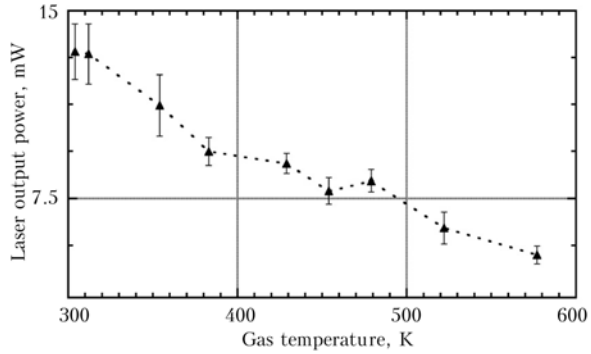

Fig. 6. Maximum power of laser output (mW) vs. gas temperature in the gas heater cell (K). The laser gas was a mixture of 76.4% Ar, 23.4% He, and 0.2% Xe with $5.50 \pm 0.15 \times10^{18}$ cm^{-3} of a constant density pumped by a 50 μs pulse. All other parameters, such as water vapor density, optical geometry, etc., were kept fixed.

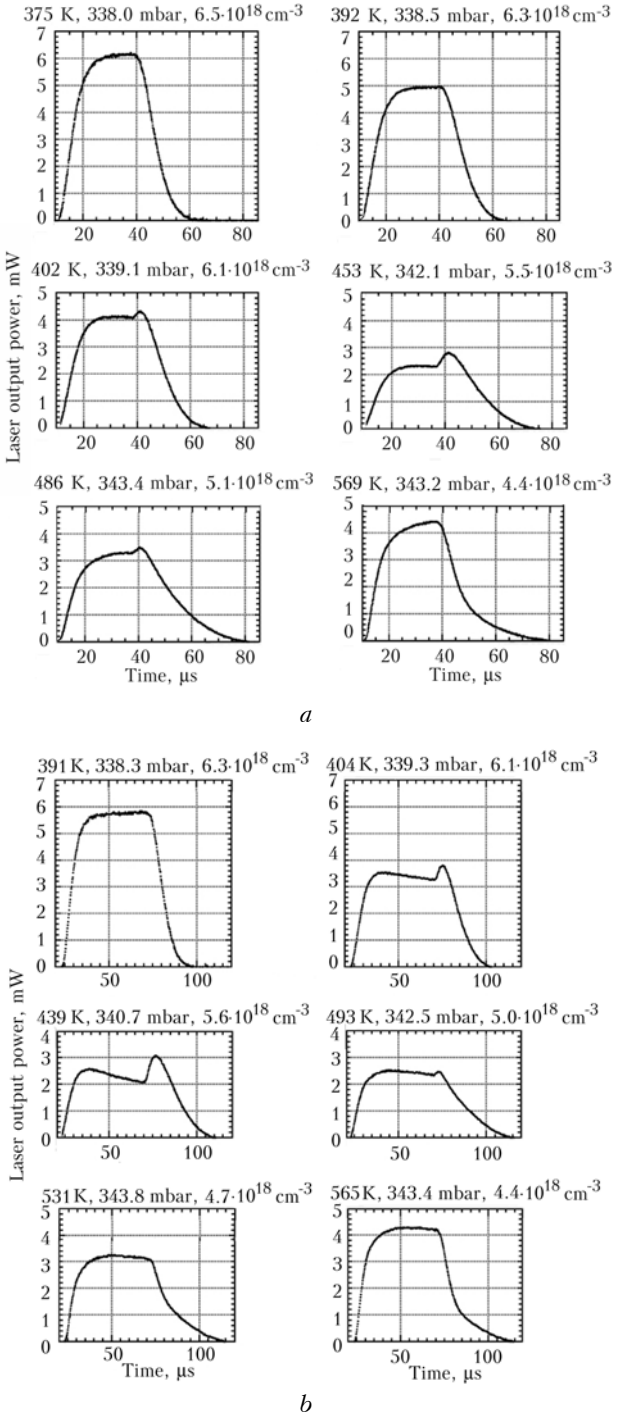

Fig. 7. Laser output power (mW) vs. time (μs) at the different gas temperatures in the gas heater cell. The laser gas was a mixture of 99.7% Ar and 0.3% Xe with 340 ± 2 mbar of a constant total gas pressure pumped by a 30 μs (*a*) and 50 μs (*b*) pulse. All other parameters, such as water vapor density, optical geometry, etc., were kept fixed.

The next run shows the laser output power pulses using a purified Ar (76.4%) – He (23.4%) – Xe (0.3%) gas mixture with 443 ± 4 mbar of a constant total gas pressure pumped by a 50 Us pulse. The data shown in Fig. 8 are several laser output power pulses at different

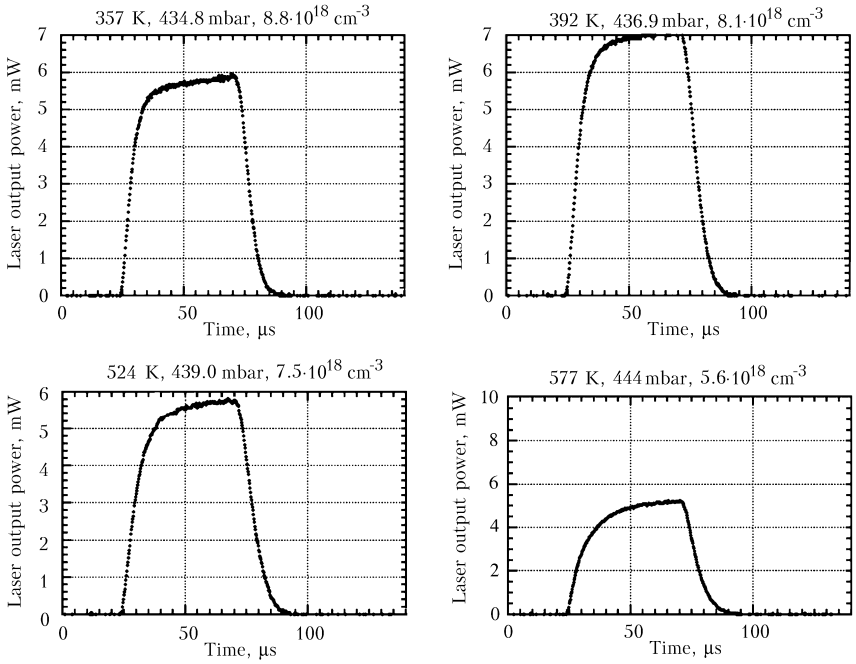

Fig. 8. Laser output power (mW) vs. time (μs) at the different gas temperatures in the gas heater cell. The laser gas was a mixture of 99.7% Ar and 0.3% Xe with 443 ± 4 mbar of a constant total gas pressure pumped by a 50 μs pulse. All other parameters, such as water vapor density, optical geometry, etc., were kept fixed.

gas temperatures in the gas heater cell. Note that the shape of the laser output pulses changes at different gas temperatures.

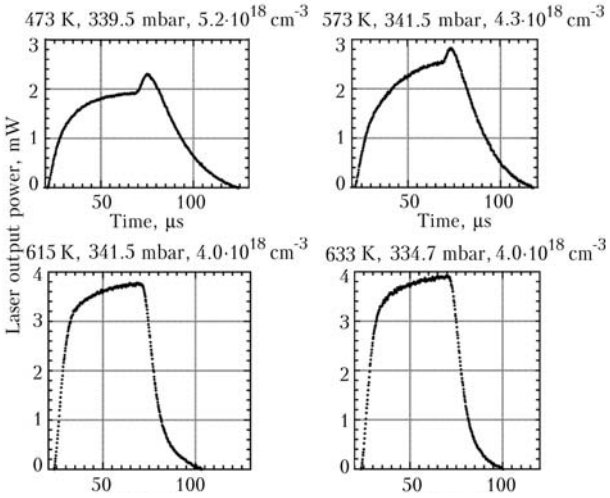

Fig. 9. Laser output power (mW) vs. time (μs) at the different gas temperatures in the gas heater cell. The laser gas was a mixture of 99.5% Ar and 0.5% Xe with 342 ± 3 mbar of a constant total gas pressure pumped by a 50 μs pulse. All other parameters, such as water vapor density, optical geometry, etc., were kept fixed.

The last run shows the laser output power pulses using a purified Ar–Xe (0.5%) gas mixture with 342 ± 3 mbar of a constant total gas pressure pumped by a 50 Us pulse. Some laser output power pulses at different gas temperatures in the gas heater cell are shown in Fig. 9. They show that the laser output pulses using a gas mixture with other xenon concentrations have afterglow parts in another temperature region.

2.2. Comparison of the time dependence of the 1.73 and 2.03 μm Xe I laser lines at high temperature

The influence of gas temperature on the laser output power of the 1.73 ($5d[3/2]_1$–$6p[5/2]_2$) and 2.03 Um ($5d[3/2]_1$–$6p[3/2]_2$) Xe I laser lines using broadband cavity has also been studied. Some competition between the lines for the Ar–Xe (1%) gas mixture at 450 ± 2 and 438 ± 6 K are observed. The laser was pumped by 20 Us ion beam pulses. The laser output power vs. gas temperature is shown in Fig. 10. The effect of competition between the lines can be described as follows: The laser effect on the 2.03 Um line started immediately with the onset of the ion beam pumping pulse. This line reached a maximum output immediately after the onset of the pulse and was then reduced significantly. In this first competition stage, the 1.73 Um line started lasing when the 2.03 Um line had reached its maximum. In the second competition stage, ordinary lasing parts of the laser pulses were observed for both lines. In this stage, the 1.73 Um line always dominated the other line. As soon as the pumping pulse terminated, the afterglow lasing part of the 1.73 Um line started, and the laser output of the

2.03 Um line vanished instantaneously. This 1.73 Um line reached its maximum and was then reduced significantly. In this final stage, the 2.03 Um line lased after the 1.73 Um line had reached its maximum. As described above, the data show the lasing competitions between lines at 1.73 and 2.03 Um and their contrary dominating effects in the ordinary and afterglow lasing parts of the laser pulses.

3. Summary and discussion

Experiments have been performed to study the atomic xenon laser at gas temperatures up to 663 K, using Ar–Xe and Ar–He–Xe gas mixtures. In this paper, we restrict ourselves to presenting the experimental results. We analyze and summarize what we observed as follows:

A. The experimental data with Ar–Xe (1.73 Um) in Fig. 4 shows a significant linear reduction of laser output power in the region up to around 400 K, and an almost constant laser output with little reduction in the region from around 400 to 600 K, with increasing gas temperature at a constant gas density.

B. The experimental data with Ar–He–Xe (1.73 Um) in Fig. 6 shows an essentially linear reduction of laser output with increasing gas temperature at a constant gas density. Comparing Figs. 4 and 6 shows that adding helium into the Ar–Xe gas mixture improved laser performance in the higher gas temperature region.

C. In the special region of gas temperatures between 392 and 553 K and gas densities between 5.0 and 6.7×10^{18} cm^{-3}, afterglow lasing appears in Ar–Xe (1.73 Um) laser pulses.

D. After adding helium, afterglow lasing could not be observed at all in the gas temperature and density region that we measured.

E. The lasing competitions between Ar–Xe laser lines at 1.73 and 2.03 Um in Fig. 10 showed their contrary dominating effects in the ordinary and afterglow lasing parts of the laser pulses.

The experimental results A to E summarized above allowed us to make the following qualitative interpretations. The comparison of results A and B suggests that the linear reduction of the laser output with increasing gas temperature in a lower temperature region is caused by increased quenching to the laser upper level by laser buffer gases. This is due to the quenching effect, that is, reductions of the decay time and cross section for stimulated emission of the laser upper level are proportional to the square root of the gas temperature, respectively. Therefore, laser output power, which is proportional to the product of the decay time and cross section for stimulated emission, shows linear reduction with increasing gas temperature.

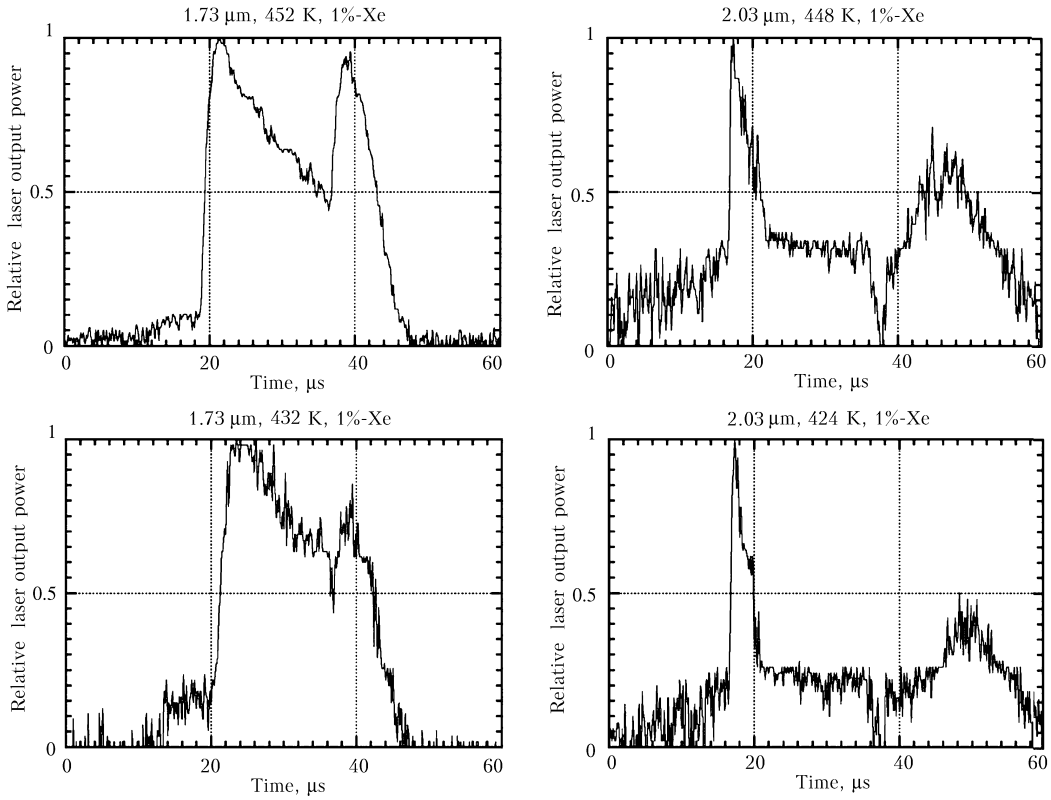

Fig. 10. Relative laser output power (mW) at 1.73 and 2.03 μm vs. time (μs) at the different gas temperatures in the gas heater cell. The laser gas was a mixture of 99% Ar and 1% Xe with the constant pressures pumped by a 20 μs pulse. All other parameters, such as water vapor density, optical geometry, etc., were kept fixed.

The difference between reduction slopes for the Ar–Xe and Ar–He–Xe gas mixtures is caused by the difference between the cross sections of quenching to the laser upper level by argon and helium. Only the Ar–Xe laser has an almost constant laser output with little reduction in the temperature region from around 400 to 600 K. This suggests that other mechanisms dominate the quenching effect by buffer gas. The mechanisms can be electron collisional mixing (ECM), because this rate increases at high electron temperatures. Helium reduces the raising of the electron temperature with its larger collisional electron cooling effect, because helium has less mass than argon. This could be a reason why the Ar–He–Xe laser does not show an almost constant reduction in its temperature region in Fig. 6.

Afterglow lasing is mainly caused by the high rate of the dissociative recombination decay to the common laser upper level at a low electron temperature and a high density. Because a higher gas temperature keeps the electron temperature higher in collisional electron cooling, a higher electron temperature lowers the rate of dissociative recombination. As a result, the laser plasma in the ordinary lasing part has a high electron temperature and density. When pumping terminates and gas temperature instantly becomes lower, the condition of the low electron temperature and high density results in a high rate of dissociative recombination. Consequently, the afterglow lasing appears just after pumping termination. Results C and D together indicate that afterglow lasing appears only in the ECM-dominated temperature region of more than around 400 K. This is the reason that afterglow lasing has not been observed at all with the added helium. This suggests that ECM also has some effect on the time structure of lasing. Additionally, result E informs us that there are complex gas kinetics in the manifold. The lasing competition between Ar–Xe laser lines at 1.73 and 2.03 Um is caused by different rate constants of electron-exciting and de-exciting in the lower levels of the laser lines at 1.73 and 2.03 Um. These rate constants have a dependence on electron temperature and density in the laser plasma. The plasma in the ordinary and afterglow lasing parts have different electron temperatures and densities. This can be caused by their contrary dominating oscillation in each lasing part.

In our experiment, the lens effect at the ends of the gas heater cell may give some influences on the laser performance in the higher gas temperature region. However, the data of the lasing competition indicates that these gas temperature effects cannot be explained by the lens effect alone. Consequently, to quantitatively explain these temperature dependences, all recombination rates, production rates of molecule ions, and electron collisional mixing rates in the manifold will have to be taken into consideration for modeling observed effects.

These experimental data show that increasing the gas temperature must be considered together with potential increasing water vapor impurities due to the outgassing of laser gas[17] as a cause for reduced laser performance in high power Ar–Xe laser systems. In order to understand high power and long pulse NPL-systems in practice, it is important to investigate NPL-problems and the mechanisms of water vapor influence on laser outputs at high temperatures. In this study, the influence of increasing gas temperature has been performed, while quantitatively controlling the other parameters, especially water vapor impurities. As a result of comparable experimental and analytical results on water vapor[17] and temperature dependence of laser intensity, dominant causes of the NPL-problems can be identified as outgassing water vapor under the conditions of NPL-experiments. These data provide important information for a precise laser gas kinetic model of NPLs and stable NPLs in operation.

Acknowledgments

This work was funded by Tandem Accelerator Laboratory Munich, NATO grant 921215, INTAS grant 96/351 and DAAD (Deutscher Akademischer Austauschdienst). Experiments were performed during H. Tomizawa's exchange program funded by DAAD. The authors acknowledge the assistance of B. Russ in designing and building the experimental setup. We also acknowledge the helpful support of the staff of Tandem Accelerator Laboratory Munich and Fakultät für Physik E12, Technische Universität München.

References

1. A.M. Voinov, L.E. Dovbysh, V.N. Krivonosov, S.P. Mel'nikov, A.T. Kazakevich, I.V. Podmoshenkii, and A.A. Sinyanskii, Sov. Phys. Dokl. **24**, 189 (1979).
2. A.V. Karelin, A.A. Sinyanskii, and S.I. Yakovlenko, Quantum Electron. **27,** 375 (1997).
3. A.M. Voinov, L.E. Dovbysh, V.N. Krivonosov, S.P. Mel'nikov, A.T. Kazakevich, I.V. Podmoshenskii, and A.A. Sinyanskii, Sov. Tech. Phys. Lett. **5**, 171 (1979).
4. O.V. Sereda, V.F. Tarasenko, A.V. Fedenev, and S.I. Yakovlenko, Quantum Electron. **23**, 459 (1993).
5. W.J. Witteman, S.W.A. Gielkens, V.N. Tskhai, and P.J. Peters, in: *Proc. of Int. Conf. on Atomic and Molecular Pulsed Lasers II,* Tomsk, Russia (1997), V.F. Tarasenko, G.V. Mayer, and G.G. Petrash, eds., Proc. SPIE, **3403**, p. 11.
6. A.V. Karelin and O.V. Simakova, Preprint No. 9, Mar. 15, 1998 (private communications).
7. G.A. Hebner and G.N. Hays, J. Appl. Phys. **65**, 3760 (1993).
8. A.V. Karelin, Quantum Electron. **28**, 602 (1998).
9. P.P. Dyachenko, in: *Proc. of the 12th Int. Conf. on Laser Interaction and Related Plasma Phenomena*, Osaka, Japan (1995), S. Nakai and G.H. Miley, eds., Osaka, Japan, 1995, ISBN 1-56396-624-7, Vol. 2, p. 894.
10. M. Ohwa and M.J. Kushner, J. Quantum Electronics **26**, 1639 (1990).
11. M. Ohwa, T.J. Moratz, and M.J. Kushner, J. Appl. Phys. **66**, 5131 (1989).

12. V.A. Ivanov, Sov. Phys. μ sp. **35**, 17 (1992).
13. G.A. Hebner and G.N. Hays, J. Appl. Phys. **74**, 3673 (1993).
14. W.J. Alford and G.N. Hays, J. Appl. Phys. **65**, 3760 (1989).
15. V.N. Kononov, M.V. Bokhovko, A.P. Budnik, I.V. Dobrovolskaya, and O.E. Kononov, in: *Proc. of the Ninth Int. Conf. on Emerging Nuclear Energy Systems,* Tel-Aviv, Israel (1998), Y. Ronen, L. Teppers, and E. Elias, eds., Vol. 2, p. 881.
16. A.A. Mavlyutov, A.I. Mis'kevich, and B.S. Salamakha, in: *Proc. of the 2nd Int. Conf. on Physics of Nuclear-Induced Plasma and Problems of Nuclear-Pumped Lasers (NPL-94),* Arzamas-16, Russia (1994), A.M. Voinov, S.P. Melnikov, and A.A. Sinyanskii, eds., VNIIEF, Arzamas-16, 1995, ISBN 5-85165-065-9, Vol. 1, p. 318.
17. H. Tomizawa, M. Salvermoser, J. Wieser, and A. μ lrich, J. Phys. B **32** (2000).
18. A.I. Konak, S.P. Melnikov, V.V. Porkhaev, and A.A. Sinyanskii, Laser and Particle Beams **11**, 663 (1993).
19. G.A. Hebner, J.W. Shon, and M.J. Kushner, Appl. Phys. Lett. **63**, 2872 (1993).
20. G.A. Hebner, IEEE J. Quantum Electronics **31**, 1626 (1995).
21. μ lrich, H. Bohn, P. Kienle, and G.J. Perlow, Appl. Phys. Lett. **42**, 782 (1983).